

Noncollinear two- and three-dimensional magnetic ordering in the honeycomb lattices of ErX_3 ($X = \text{Cl}, \text{Br}, \text{I}$)

K. W. Krämer and H. U. Güdel

Department for Chemistry and Biochemistry, University of Bern, Freiestrasse 3, CH-3000 Bern 9, Switzerland

B. Roessli and P. Fischer

Laboratory for Neutron Scattering, Paul Scherrer Institute and ETH Zürich, CH-5232 Villigen PSI, Switzerland

A. Dönni

Department of Physics, Niigata University, Niigata 950-2181, Japan

N. Wada

Institute of Physics, Graduate School of Arts and Sciences, University of Tokyo, Tokyo 153-8902, Japan

F. Fauth and M. T. Fernandez-Diaz

Institute Laue-Langevin, Boîte Postale 156, F-38042 Grenoble Cedex 9, France

T. Hauss

Hahn-Meitner Institute, Glienicke Strasse 100, D-14109 Berlin, Germany

(Received 13 April 1999)

Unusual magnetic ordering phenomena have been observed in the three title compounds in the milli-Kelvin temperature range. The ratio of interlayer to intralayer coupling and thus the critical behavior and the nature of the magnetic order can be tuned by chemical variation. In all three lattices the two-dimensional (2D) magnetic order within the layers is a two sublattice 120° antiferromagnetic order with an infinite rotational degeneracy. The ordered magnetic moments increase from 3.3 to 4.7 and $5.5\mu_B/\text{Er}^{3+}$ for ErCl_3 , ErBr_3 , and ErI_3 , respectively. ErCl_3 shows a transition to 3D magnetic order at 350 mK with a \mathbf{k} vector of $(\frac{2}{3}, 0, -\frac{1}{12})$. ErBr_3 and ErI_3 are the first examples of rare-earth trihalides displaying short-range 2D magnetic order from 400 mK up to several Kelvin, long-range 2D order between 280 mK and 400 mK, long-range 2D and short-range 3D order with $\mathbf{k} = (\frac{1}{3}, \frac{1}{3}, 0)$, and a correlation length of 15 \AA below 280 mK. The differences are attributed to the different layer stackings in ErCl_3 and $\text{ErBr}_3/\text{ErI}_3$ as well as the variation of interlayer distances. [S0163-1829(99)50530-4]

Competing interactions in low-dimensional magnetic systems often lead to unusual magnetic ordering and critical phenomena.¹ The simple binary systems ErX_3 ($X = \text{Cl}, \text{Br}, \text{I}$) constitute a particularly interesting family of insulating compounds with closely related layer structures. The competition between intra- and interlayer interactions can be influenced by the variation of X . The magnetic order and critical behavior derived from neutron-diffraction and heat-capacity measurements in the milli-Kelvin temperature range is unusual. Common to all three compounds is a 2D magnetic order within the honeycomb layers. Whereas ErCl_3 undergoes a transition to 3D magnetic order at 350 mK as a result of interlayer interactions, ErBr_3 and ErI_3 exhibit most unusual phenomena below 400 mK. The ordering temperature of ErCl_3 is in reasonable agreement with $T_N = 307 \text{ mK}$ determined from a single-crystal susceptibility measurement.² In this paper we present results on the magnetic order in this class of insulating antiferromagnets. The data are quantitatively analyzed and the results qualitatively discussed.

ErCl_3 and ErBr_3 were prepared from Er_2O_3 following the NH_4X synthetic route,³ whereas ErI_3 was synthesized from Er and I_2 according to Ref. 4. All three compounds are highly hygroscopic, therefore all storage and handling was

done in a glove box ($\text{H}_2\text{O} < 0.1 \text{ ppm}$). All samples were sublimed in evacuated silica containers at 700°C for purification. Single crystals were grown by the Bridgman technique. Powder neutron measurements were done at the D1A and D1B diffractometers at the Institute Laue-Langevin (ILL) in Grenoble. Single-crystal neutron diffraction was done at the V1 diffractometer of the Hahn-Meitner Institute (HMI) in Berlin. The heat-capacity measurement of an ErBr_3 crystal was performed at the University of Tokyo. For all measurements the samples were cooled in $^3\text{He}/^4\text{He}$ dilution cryostats. The crystal structure of ErCl_3 (AlCl_3 -type structure)⁵ is monoclinic, space group $C2/m$, with lattice parameters of $a = 6.8040(3) \text{ \AA}$, $b = 11.7456(5) \text{ \AA}$, $c = 6.3187(3) \text{ \AA}$, and $\beta = 110.851(3)^\circ$ at 1.5 K. The Cl^- ions form a slightly distorted cubic densest packing of spheres with the Er^{3+} ions occupying $\frac{2}{3}$ of the octahedral voids of every other layer in an ordered way. This results in ErCl_3 layers parallel to the a - b plane and stacked along the c axis. In ErBr_3 and ErI_3 (BiI_3 -type structure)⁶ the halide ions form a hexagonal densest packing of spheres. As in ErCl_3 $\frac{2}{3}$ of the octahedral voids of every other layer are occupied by Er^{3+} , but the layer stacking along the c axis is different. The space group is $R\bar{3}$ and the unit cell dimensions at 1.5 K are $a = 7.0051(2) \text{ \AA}$, $c = 18.8940(7) \text{ \AA}$ for ErBr_3 , and $a = 7.4024(1) \text{ \AA}$, c

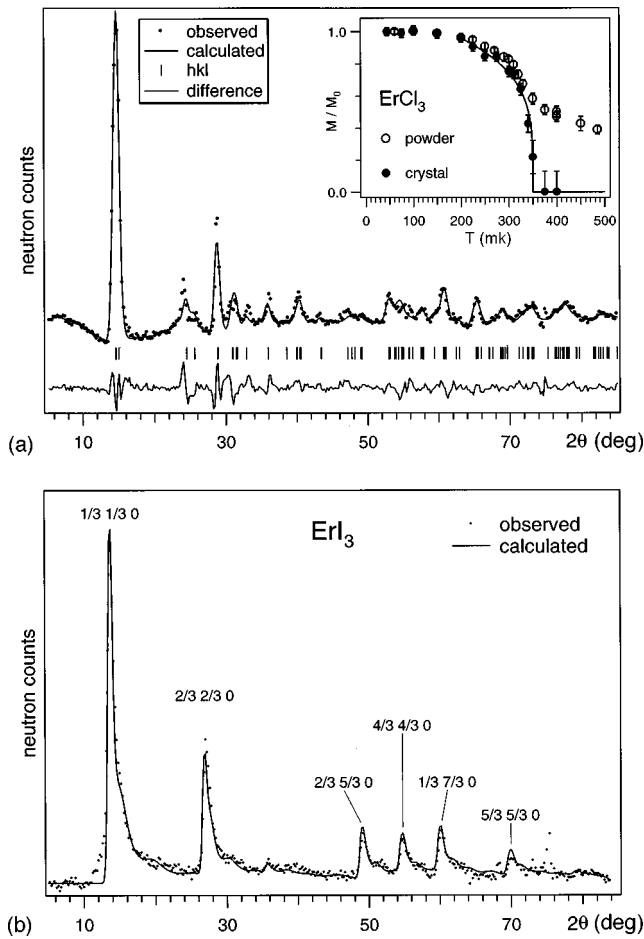


FIG. 1. Neutron powder diffraction difference diagrams (a) 60–485 mK of ErCl_3 and (b) 20–800 mK of ErI_3 (D1B, $\lambda = 2.52 \text{ \AA}$). The normalized square root of the intensity of the magnetic peak at $2\theta = 15^\circ$ as well as that of the $(-\frac{2}{3}, 0, \frac{1}{12})$ single-crystal reflection of ErCl_3 is shown as a function of temperature as an inset in (a). In (b) the strongest magnetic reflections are denoted by their hkl values. The full lines in both figures correspond to least-squares fits explained in the text.

$= 20.6020(9) \text{ \AA}$ for ErI_3 . As a result of the 2D character of the structures the crystals easily cleave parallel to the layers.

Figures 1(a) and 1(b) show neutron-diffraction difference diagrams, 60–485 mK and 20–800 mK for ErCl_3 and ErI_3 , respectively. ErBr_3 exhibits very similar diffraction behavior to ErI_3 in this temperature range. In these difference diagrams the contributions from nuclear scattering are to a good approximation eliminated, and we are left with the pure magnetic neutron-diffraction pattern. The ErI_3 diagram essentially consists of six asymmetric peaks with intensity modulations towards higher angle for each peak. The six features can also be recognized as dominant peaks in the ErCl_3 pattern, but here they are not asymmetric, and there are numerous additional lines. The intensity of the peak at $2\theta = 15^\circ$ as well as that of the $(-\frac{2}{3}, 0, \frac{1}{12})$ single-crystal reflection are shown as a function of temperature as an inset in Fig. 1(a). From a fit of Eq. (1) to the single-crystal data a critical exponent $\beta = 0.23(2)$ is obtained, which is intermediate between the β values of 0.125 and 0.325 for pure 2D and 3D Ising systems, respectively.⁷

TABLE I. Magnetic structures of ErCl_3 and $\text{ErBr}_3/\text{ErI}_3$. The Néel temperature T_N is given for the onset of the 3D order. μ denotes the ordered magnetic moment per Er^{3+} at saturation.

	ErCl_3	ErBr_3	ErI_3
T_N/mK	350	280	280
μ/μ_B	3.3(1)	4.7(2)	5.5(2)
\mathbf{k} vector	$(\frac{2}{3}, 0, -\frac{1}{12})$	$(\frac{1}{3}, \frac{1}{3}, 0)$	$(\frac{1}{3}, \frac{1}{3}, 0)$

$$\frac{M}{M_0} = \left(1 - \frac{T}{T_N}\right)^\beta. \quad (1)$$

The nonvanishing magnetic intensity in the powder data above $T_N = 350(5) \text{ mK}$ (see inset Fig. 1) is the result of considerable short-range magnetic order. The magnetic structure of ErCl_3 was solved using the powder data and the FULLPROF program.⁸ The result of the best fit is included as a full line in Fig. 1(a) and the corresponding parameter values are listed in Table I. The magnetic order within the layers can be represented by the two sublattice structure shown in Fig. 2(a). Each sublattice forms a triangular 120° antiferromagnetic structure. The magnetic ordering vector $\mathbf{k} = (\frac{2}{3}, 0, -\frac{1}{12})$ was determined from a single-crystal measurement. It is temperature independent and commensurate. The component of the \mathbf{k} vector along the c^* axis leads to a rotation of the magnetic moments in the a - b plane of 30° from layer to layer.

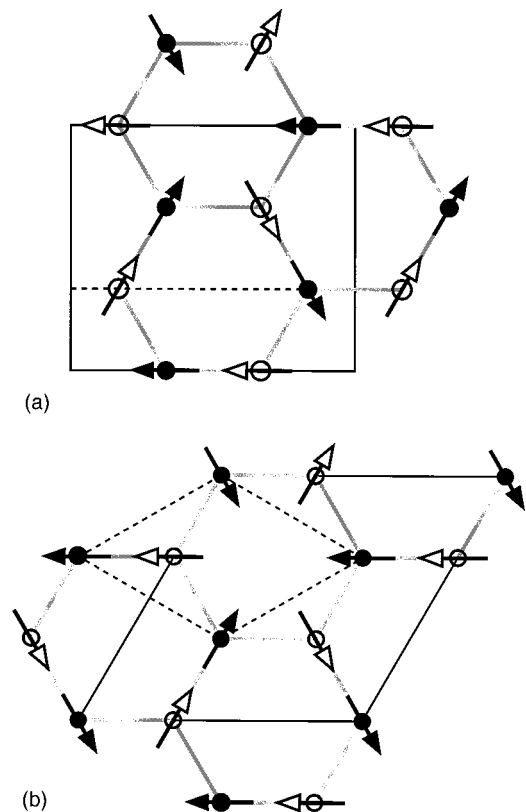


FIG. 2. 2D magnetic structures within the crystallographic layers of (a) ErCl_3 , $\mathbf{k} = (\frac{2}{3}, 0, -\frac{1}{12})$ and (b) $\text{ErBr}_3/\text{ErI}_3$, $\mathbf{k} = (\frac{1}{3}, \frac{1}{3}, 0)$. The dashed and full lines denote the crystallographic and magnetic unit cells, respectively.

Figure 2(b) shows the 2D order of the magnetic moments for the rhombohedral ErBr_3 and ErI_3 lattices. The motif is the same as in Fig. 2(a), and in the rhombohedral cell the ordering vector is $\mathbf{k} = (\frac{1}{3}, \frac{1}{3}, 0)$. This was derived from a fit to the relative intensities of the six magnetic reflections in Fig. 1(b) and directly confirmed by single-crystal investigations.

This basic 2D magnetic order of ErCl_3 as well as $\text{ErBr}_3/\text{ErI}_3$ has the remarkable property that it is infinitely degenerate. Rotation of the spins of one sublattice by any angle φ within the a - b plane coupled to a rotation of the second sublattice by $-\varphi$ leads to an equivalent structure with the same energy. This behavior is comparable to the infinite degeneracy of the magnetic ground state of solid oxygen in its rhombohedral β -phase.⁹ Except for this triangular lattice of solid oxygen we are not aware of any experimental manifestation of such a phenomenon.

A comparable 2D magnetic structure has been reported for the intermetallic compound UNi_4B .¹⁰ However, in this system there is a paramagnetic uranium atom in the center of each hexagon of Fig. 2(b). Furthermore, the magnetic interactions in this metallic system with short U-U distances and small magnetic moments are physically very different from those in the insulating ErX_3 halides with long Er-Er separations and large magnetic moments. In contrast to our structure the magnetic structure factors of UNi_4B were found to depend on a rotation within the plane.

The asymmetric shape of the magnetic reflections with the intensity modulation towards larger scattering angles of ErI_3 in Fig. 1(b) is typical of a system with magnetic order in two dimensions and short-range order in the third direction. Similar peak shapes have been observed for graphite¹¹ and in the magnetic peaks of rare earth containing layer-type cuprate superconductors.¹² The information contained in the intensity and shape of the magnetic peaks in Fig. 1(b) was used to extract the correlation length in the third dimension and the value and orientation of the ordered Er moments within the plane. We used the formalism introduced in Ref. 13 for a fit to the experimental data at 20 mK and obtained a correlation length along the c axis of $15(3)$ Å for both ErBr_3 and ErI_3 , and ordered magnetic moments of $\mu = 4.7(2)\mu_B$ and $5.5(2)\mu_B$ for ErBr_3 and ErI_3 , respectively. The best fits were obtained for the magnetic-moment orientation perpendicular to the c axis. The calculated profile for ErI_3 is included as a full line in Fig. 2(b). The correlation length of 15 Å roughly corresponds to the distance between adjacent layers, i.e., $\frac{2}{3}$ the c axis.

This peculiar magnetic ordering is also reflected in the critical behavior, which is shown for ErBr_3 in Fig. 3. First we notice that the temperature dependence of the ordered magnetic moment is distinctly different from the behavior of ErCl_3 [inset Fig. 1(a)]. For the single-crystal magnetization (Fig. 3, middle) no saturation of the ordered magnetic moment is observed down to 60 mK, as expected for a 2D magnetic structure with stacking disorder in the third dimension. From the linewidth of the $(\frac{1}{3}, \frac{1}{3}, 0)$ magnetic reflection (Fig. 3, bottom) one can very clearly distinguish three temperature ranges corresponding to different ordering regimes of the magnetic moments. This is indicated by the dashed vertical lines in Fig. 3. The range above 400 mK up to several Kelvin is characterized by short-range magnetic order

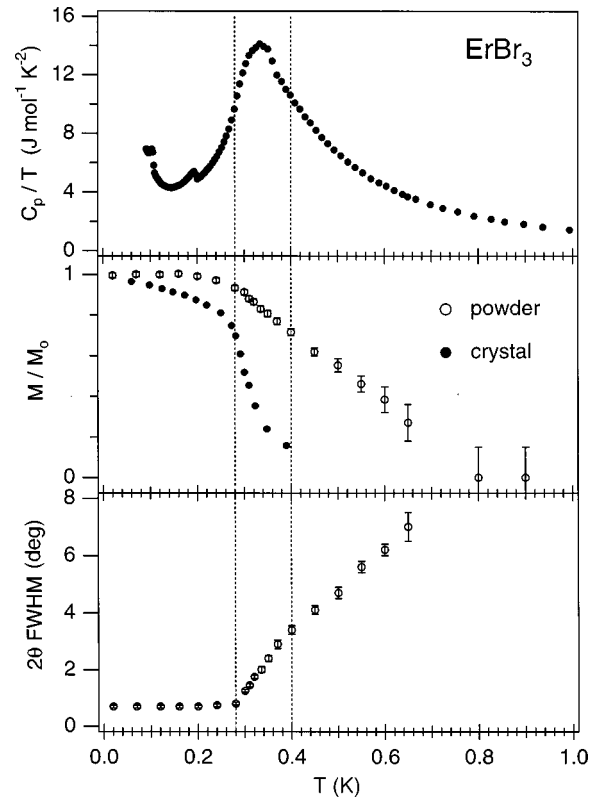


FIG. 3. Critical behavior of ErBr_3 . Top: heat capacity, middle: normalized square root of the intensity of the magnetic peak at $2\theta = 14^\circ$ from powder [see Fig. 1(b)] and single-crystal data, and bottom: linewidth of the magnetic peak at $2\theta = 14^\circ$ are shown as a function of temperature. The dashed lines separate the following physical regimes: above 400 mK: short-range 2D order, 280–400 mK: long-range 2D order, and below 280 mK: 3D correlation.

within the layers, between 400 and 280 mK long-range 2D magnetic order within the layers sets in, and below 280 mK the 3D correlation with a length of 15 Å is established. From the magnetic heat capacity (Fig. 3, top) we see that less than 20% of the magnetic entropy loss occurs below 280 mK, i.e., due to 3D ordering. The bulk of the magnetic heat capacity is due to the short- and long-range 2D ordering. The difference in the magnetic ordering and critical behavior between ErCl_3 on the one hand and $\text{ErBr}_3/\text{ErI}_3$ on the other can be attributed to the different geometrical stacking of the layers in the crystal structures. In ErCl_3 each Er^{3+} has four neighbor Er^{3+} ions at distances of 2×6.319 Å and 2×6.330 Å in the two adjacent layers. Magnetically, two of these neighbors belong to one sublattice and two to the other sublattice, and there is no ambiguity in the relative orientation of the magnetic moments from layer to layer. In ErBr_3 and ErI_3 , on the other hand, there is only one neighbor at a distance of 6.292 Å or 6.786 Å in one of the adjacent layers. Magnetically, this neighbor belongs to the other sublattice, but in contrast to ErCl_3 , there is a degree of freedom in the relative orientation of the magnetic moments in this pair in $\text{ErBr}_3/\text{ErI}_3$. The situations with angles of 60° , 180° , and -60° in the projection along the c axis between the two sublattices are physically equivalent. This is likely to lead to disorder in the magnetic stacking of the layers, exactly as observed.

Financial support by the Swiss National Science Foundation is gratefully acknowledged.

- ¹L. J. de Jounge and A. R. Miedema, *Experiments on Simple Magnetic Model Systems* (Taylor & Francis, London, 1974).
- ²C. W. Fairall, J. A. Cowen, and E. Grabowski, *Phys. Lett.* **35A**, 405 (1971).
- ³G. Meyer, *Inorg. Synth.* **25**, 146 (1989).
- ⁴G. Meyer, in *Synthesis of Lanthanide and Actinide Compounds*, edited by G. Meyer and L. R. Morss (Kluwer Academic Publishers, Dordrecht, 1991), p. 140.
- ⁵D. H. Templeton and G. F. Carter, *J. Phys. Chem.* **58**, 940 (1954).
- ⁶D. Brown, S. Fletcher, and D. G. Holah, *J. Chem. Soc. A* **2**, 1889 (1968); L. B. Asprey, T. K. Keenan, and F. H. Kruse, *Inorg. Chem.* **3**, 1137 (1964).
- ⁷W. Gebhardt and U. Krey, *Phasenübergänge und Kritische Phänomene* (Vieweg, Braunschweig, 1980), p. 76.
- ⁸J. Rodriguez-Carvajal, *Physica B* **192**, 55 (1993).
- ⁹E. Rastelli and A. Tassi, *J. Phys. C* **19**, L423 (1986).
- ¹⁰S. A. M. Mentink, A. Drost, G. J. Niewenhuys, E. Frikkee, A. A. Menovsky, and J. A. Mydosh, *Phys. Rev. Lett.* **73**, 1031 (1994).
- ¹¹B. E. Warren, *Phys. Rev.* **59**, 693 (1941).
- ¹²B. Roessli, P. Fischer, U. Staub, M. Zolliker, and A. Furrer, *J. Appl. Phys.* **75**, 6337 (1994); B. Roessli, P. Fischer, M. Zolliker, P. Allenspach, J. Mesot, U. Staub, A. Furrer, E. Kaldis, B. Bucher, J. Karpinski, E. Jilek, and H. Mutka, *Z. Phys. B* **91**, 149 (1993).
- ¹³O. Elsenhans, *J. Appl. Crystallogr.* **23**, 73 (1990).